Naval Research Laboratory

Washington, DC 20375-5320

NRL/MR/6703--15-9646

Atmospheric Propagation and Combining of High-Power Lasers

W. Nelson

University of Maryland
College Park, Maryland

Phillip Sprangle

Directed Energy Physics
Plasma Physics Division

C.C. Davis

University of Maryland
College Park, Maryland

September 8, 2015

REPORT DOCUMENTATION PAGE

Form Approved
OMB No. 0704-0188

1. REPORT DATE *(DD-MM-YYYY)*	2. REPORT TYPE	3. DATES COVERED *(From - To)*
08-09-2015	Interim	August 2014 – August 2015

4. TITLE AND SUBTITLE

Atmospheric Propagation and Combining of High-Power Lasers

5a. CONTRACT NUMBER

5b. GRANT NUMBER

5c. PROGRAM ELEMENT NUMBER

6. AUTHOR(S)

W. Nelson,* P. Sprangle, and C.C. Davis*

5d. PROJECT NUMBER
67-4374-C4

5e. TASK NUMBER

5f. WORK UNIT NUMBER

7. PERFORMING ORGANIZATION NAME(S) AND ADDRESS(ES)

Naval Research Laboratory
4555 Overlook Avenue, SW
Washington, DC 20375-5320

8. PERFORMING ORGANIZATION REPORT NUMBER

NRL/MR/6703--15-9646

9. SPONSORING / MONITORING AGENCY NAME(S) AND ADDRESS(ES)

Naval Research Laboratory
4555 Overlook Avenue, SW
Washington, DC 20375-5320

10. SPONSOR / MONITOR'S ACRONYM(S)

NRL

11. SPONSOR / MONITOR'S REPORT NUMBER(S)

12. DISTRIBUTION / AVAILABILITY STATEMENT

Approved for public release; distribution is unlimited.

13. SUPPLEMENTARY NOTES

*Department of Electrical and Computer Engineering, University of Maryland, College Park, MD 20740

14. ABSTRACT

In this paper we analyze the beam combining and atmospheric propagation of high-power lasers for directed-energy (DE) applications. The large linewidths inherent in high-power fiber, and to a lesser extent, slab lasers cause random phase and intensity fluctuations occurring on sub-nanosecond time scales. To coherently combine these high-power lasers would involve instruments capable of precise phase control and operating at rates greater than ~10 GHz. To the best of our knowledge, this technology does not currently exist. This presents a challenging problem when attempting to phase-lock high-power lasers, which is not encountered when phase-locking low-power lasers, for example mW power levels. Regardless, we demonstrate that even if instruments are developed that can precisely control the phase of high-power lasers; coherent combining is problematic for DE applications. The dephasing effects of atmospheric turbulence typically encountered in DE applications will degrade the coherent properties of the beam before it reaches the target. Through simulations, we find that coherent beam combining in moderate turbulence and multi-km propagation distances has little advantage over incoherent combining. Additionally, in strong turbulence and multi-km propagation ranges, we find nearly indistinguishable intensity profiles and virtually no difference in the energy on the target between coherently and incoherently combined laser beams. Consequently, we find that coherent beam combining at the transmitter plane is ineffective under typical atmospheric conditions.

15. SUBJECT TERMS

Turbulence
Beam combining
High power lasers
Directed energy

16. SECURITY CLASSIFICATION OF:			17. LIMITATION OF ABSTRACT	18. NUMBER OF PAGES	19a. NAME OF RESPONSIBLE PERSON
a. REPORT	b. ABSTRACT	c. THIS PAGE			Phillip Sprangle
Unclassified Unlimited	Unclassified Unlimited	Unclassified Unlimited	Unclassified Unlimited	27	19b. TELEPHONE NUMBER *(include area code)* (202) 767-3493

Standard Form 298 (Rev. 8-98)
Prescribed by ANSI Std. Z39.18

Atmospheric Propagation and Combining of High-Power Lasers

W. Nelson[1], P. Sprangle, and C.C. Davis[1]

Naval Research Laboratory, Plasma Physics Division
Washington, DC 20375-5346

[1]Department of Electrical and Computer Engineering, University of Maryland,
College Park, Maryland 20740

Abstract

In this paper we analyze the beam combining and atmospheric propagation of high-power lasers for directed-energy (DE) applications. The large linewidths inherent in high-power fiber, and to a lesser extent, slab lasers cause random phase and intensity fluctuations occurring on sub-nanosecond time scales. To coherently combine these high-power lasers would involve instruments capable of precise phase control and operating at rates greater than ~10 GHz. To the best of our knowledge, this technology does not currently exist. This presents a challenging problem when attempting to phase-lock high-power lasers, which is not encountered when phase-locking low-power lasers, for example mW power levels. Regardless, we demonstrate that even if instruments are developed that can precisely control the phase of high-power lasers; coherent combining is problematic for DE applications. The dephasing effects of atmospheric turbulence typically encountered in DE applications will degrade the coherent properties of the beam before it reaches the target. Through simulations, we find that coherent beam combining in moderate turbulence and multi-km propagation distances has little advantage over incoherent combining. Additionally, in strong turbulence and multi-km propagation ranges, we find nearly indistinguishable intensity profiles and virtually no difference in the energy on the target between coherently and incoherently combined laser beams. Consequently, we find that coherent beam combining at the transmitter plane is ineffective under typical atmospheric conditions.

Manuscript approved August 18, 2015.

I. Introduction

Advances in solid state lasers, especially slab and fiber lasers, have made them candidates for directed-energy applications [1,2]. To achieve the power levels needed for these applications it is necessary to combine a large number of lasers into a single beam. The combined beam is then propagated many kilometers through a turbulent atmosphere. Recently, much effort has been expended in coherent beam combining [2-7]. Coherent beam combining refers to matching the phases of multiple lasers either in the transmitter plane [2,3] or the target plane [4]. However, there are a number of important issues to be considered before a coherent combining architecture can be used for DE applications. These issues include the consideration of sources with a finite spectral linewidth and the dephasing effect of atmospheric turbulence.

Coherent combining has proven to be effective in situations with very low-power lasers and weak turbulence [4]. However, these conditions are not applicable for DE systems which require high-power lasers and must be effective in conditions of moderate and strong atmospheric turbulence. High-power fiber lasers have significantly broader linewidths due to stimulated Brillouin scattering, Doppler shift, self-phase modulation, and Raman broadening in the gain medium. Stimulated Brillouin scattering (SBS) is the main contributor to the large linewidths in high-power fiber lasers. The SBS instability results in a threshold power level for fiber and slab lasers. To increase the threshold power level, the linewidth is intentionally broadened.

The full width half max (FWHM) of the linewidth for high-power fiber lasers (multi-kW) is typically $\Delta\upsilon \approx 10\,\mathrm{GHz}$ and the coherence time is $t_C \sim 1/\Delta\upsilon = 0.1\,\mathrm{nsec}$ (for all single peaked lineshapes) [9]. Phase locking of lasers requires measuring the output phase information and applying the corrective phase to the individual lasers. To be effective, the time scale required for this process should be less than the laser coherence time. The coherence time is the characteristic time over which the phase and intensity randomly vary and is due solely to the finite spectral linewidth in the gain medium and the statistical nature of the emission from the atoms or molecules [8]. Stated simply, if the process of measuring the output phase and applying the corrective phase takes longer than the coherence time, then the output phase has changed before the corresponding corrective phase can be applied. To the best of our knowledge, there do not currently exist instruments that can operate at rates comparable to the FWHM of the linewidth for high-power fiber lasers. However, in the following work we assume that there exist

instruments that can control the phase over time scales shorter than $t_C \approx 1/\Delta\upsilon = 0.1\text{nsec}$. Furthermore, we assume that these instruments operate with zero error.

As previously stated, the power spectral linewidth associated with the gain medium results in temporal fluctuations of the intensity and phase at the output. The nature of the temporal fluctuations depends on the shape of the power spectral linewidth. As shown in Appendix B, the fluctuations associated with a Lorentzian power spectral density are characteristically different than the fluctuations associated with a Gaussian power spectral density due to the extended wings of the Lorentzian spectrum. A Lorentzian spectrum can result from collisional broadening, while a Gaussian spectrum can result from Doppler broadening or local random atom environments in a solid. Regardless of the lineshape, the standard deviation of intensity is approximately equal to the average intensity. In addition, the output phase of the field randomly fluctuates over 2π radians on time scales down to the coherence time. Experimental observations on the lineshapes of high-power fiber lasers have revealed lineshapes that are approximately Lorentzian.

In this paper we discuss the physical processes associated with the combining and propagation of high-power laser beams. We compare the energy delivered to a target for the case of coherently combined and incoherently combined laser beams. Through simulation, we demonstrate that in vacuum and weak turbulence, the effectiveness of coherent combining is limited by the phase fluctuations occurring due to the broad linewidth of high-power lasers (Figures 2 and 3). Furthermore, the advantages of coherent combining begin to diminish in moderate turbulence, as the turbulence induced phase distortions become dominant (Figures 5 and 6). In strong turbulence and multi-km propagation ranges, we find negligible differences in the energy on the target between coherently and incoherently combined laser beams (Figures 7 and 8). The incoherently combined architecture is far simpler to implement and both beam combining architectures have the capability of employing adaptive optics to extend the range.

We begin in Section II by describing the model for the beam director. We present our propagation simulation results in Section III for weak, moderate, and strong turbulence. A discussion of our findings concludes this paper in Section IV.

II. Beam Director Model

We model the beam director as a set of nine square beams which we refer to as tiles. The side length of each tile is a and the distance between the centers of adjacent tiles is b where $b \geq a$. For example, a beam director with the parameters a=b would have no filling factor and appear as a single tile with side length 3a and centered at $(x=0, y=0)$. The tile arrangement in the xy plane is shown in Fig. 1a. Tiles are indexed by the indices l and m corresponding to the x and y dimensions respectively. Indices l and m are integers defined on the set $\{-1,0,1\}$. For example, the indices $(l=-1, m=-1)$, $(l=0, m=0)$, and $(l=1, m=1)$ correspond to the bottom left, center, and top right tiles respectively.

Figure 1b shows a side view of the beam director, i.e. yz plane. Each tile is positioned with tip-tilt correction so that the center of the tile propagates to the point $(x=0, y=0, z=L)$ in vacuum where L is the distance from transmitter to the target and $L \gg b$. The tilt applied to a tile with index m is defined as $\varphi_y = mb/L$. Similarly the tip applied to a tile with index l is defined as $\varphi_x = lb/L$.

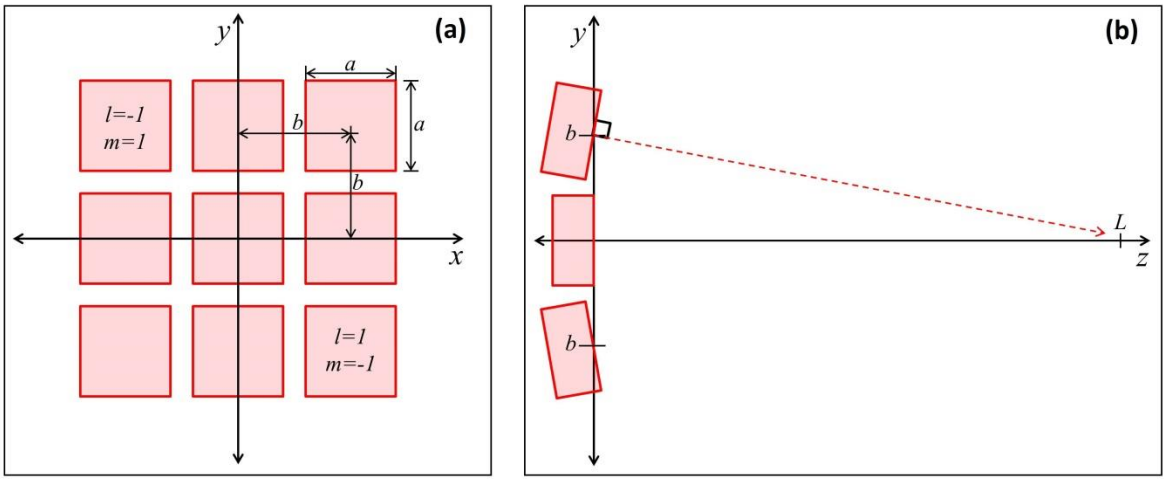

Figure 1: Beam director geometry. We define the side length of each tile as a and the distance between the centers of adjacent tiles as b where $b \geq a$. Each tile is indexed by the indices l and m defined on the set $\{-1,0,1\}$.

We follow the method presented in [10] and [11] for generation of a laser beam with arbitrary spectral power density. The method entails modeling the beam as radiation from a large number of independent radiators that radiate at discrete frequencies. We consider radiation from a total of N frequencies and write the n^{th} frequency as $\omega_n = \omega_0 + n\delta\omega$, where ω_0 is the center frequency, $\delta\omega$

is a small change in frequency, and n is an integer value ranging from $-N/2$ to $N/2-1$. The time dependence of the electric field for a single frequency ω_n can be written as

$$E_n(t) = \tfrac{1}{2}(a_n + ib_n)e^{-i\omega_n t} + \text{c.c.}, \tag{1}$$

where a_n and b_n are random variables. As a consequence of the central limit theorem, a_n and b_n are Gaussian random variables with zero mean and variance proportional to the number of radiators at frequency ω_n, which is determined by the power spectrum of radiation. The implications of Gaussian and Lorentzian power spectra are discussed in Appendices A and B. The time dependence of the total electric field from all frequency components is

$$E(t) = \sum_n E_n(t) = \tfrac{1}{2}\sum_n (a_n + ib_n)e^{-i\omega_n t} + \text{c.c.}. \tag{2}$$

Setting $\omega_n = \omega_0 + n\delta\omega$, the total electric field is given by

$$E(t) = \tfrac{1}{2}\exp[-i\omega_0 t]\sum_n (a_n + ib_n)\exp[-in\delta\omega t] + \text{c.c.}. \tag{3}$$

The term $\sum_n (a_n + ib_n)e^{-in\delta\omega t}$ is a time dependent complex value. We denote this value as $\alpha(t) + i\beta(t)$:

$$\alpha(t) + i\beta(t) = \sum_{n=-N/2}^{N/2-1} (a_n + ib_n)\exp[-in\delta\omega t]. \tag{4}$$

Numerically, t is a sequence of discrete values such that $t = m\delta t$ where m is an integer value ranging from 0 to N-1 and δt is to be determined.

$$\alpha(m\delta t) + i\beta(m\delta t) = \sum_{n=-N/2}^{N/2-1} (a_n + ib_n)\exp[-inm\delta\omega\delta t]. \tag{5}$$

If we choose $\delta t = 2\pi/(N\delta\omega)$, we get the exact definition of a discrete Fourier transform (DFT)

$$\alpha(m\delta t) + i\beta(m\delta t) = \sum_{n=-N/2}^{N/2-1} (a_n + ib_n)\exp[-i2\pi nm/N] \tag{6}$$

Thus it is convenient to solve for $\alpha(t)$ and $\beta(t)$ with the use of a DFT on the sequence $(a_n + ib_n)$ where α and β are the real imaginary part of the resulting DFT respectively. The total electric field can be written as an amplitude and phase modulated monochromatic source

$$E(t) = \tfrac{1}{2}\left(\alpha(t) + i\beta(t)\right)\exp[-i\omega_0 t] + \text{c.c.}. \tag{7}$$

Combining the time dependence described by Eq. (7) with the spatial geometry of the beam director, we write the electric field of a single tile as

$$E_{l,m}(x,y,z=0,t) = \tfrac{1}{2}\left(\alpha_{l,m}(t)+i\beta_{l,m}(t)\right)\mathrm{rect}(x-lb)\,\mathrm{rect}(y-mb) \times E_0 e^{-ik_0(y-mb)\varphi_y} e^{-ik_0(x-lb)\varphi_x} e^{-i\omega_0 t} + \text{c.c.} \tag{8}$$

where $\mathrm{rect}(\zeta)$ is the rectangular function defined as

$$\mathrm{rect}(\zeta) = \begin{cases} 0 & \text{if } |\zeta| > a/2 \\ 1/2 & \text{if } |\zeta| = a/2 \\ 1 & \text{if } |\zeta| < a/2 \end{cases} \tag{9}$$

The electric field of the beam director is obtained by summing over all tiles:

$$E(x,y,z=0,t) = \sum_{l=-1}^{l=1}\sum_{m=-1}^{m=1} \tfrac{1}{2}\left(\alpha_{l,m}(t)+i\beta_{l,m}(t)\right)\mathrm{rect}(x-lb)\,\mathrm{rect}(y-mb) \times E_0 e^{-ik_0(y-mb)\varphi_y} e^{-ik_0(x-lb)\varphi_x} E_0 e^{-i\omega_0 t} + \text{c.c} \tag{10}$$

In theory, two coherently combined tiles would have a phase difference of zero at any instance in time. However, in practice this is generally not the case for high-power lasers. Instead, coherent combining systems result in a reduction of the root mean square (RMS) phase difference between tiles. For reference, the RMS phase difference between two incoherently combined tiles is $2\pi/\sqrt{12}$ as shown in Appendix C. To simulate a situation where the tiles are coherently combined in the transmitter plane, we generate a set of $\alpha_{l,m}(t)$ and $\beta_{l,m}(t)$ in which the RMS phase difference between any two tiles can be precisely controlled. This procedure for generating a set of correlated $\alpha_{l,m}(t)$ and $\beta_{l,m}(t)$ is described in Appendix C.

III. Propagation in Turbulent Atmosphere

We simulate the propagation of the tile arrangement described in Section II through the atmosphere for coherently and incoherently combined tiles. For comparison, we include the case of monochromatic, phase matched tiles. Following our previous work [12], we propagate the beam by numerically solving the paraxial wave equation. Atmospheric turbulence is modeled as phase screens located at discrete locations along the z-axis. For details on the split-step phase screen simulation see [12].

We use parameters that are typical for DE applications. Specifically, the center wavelength of radiation in vacuum $\lambda_0 = 1\mu\text{m}$, distance to the target $L = 5\text{ km}$, tile side length $a = 2\text{ cm}$, distance between tile centers $b = 2.2\text{ cm}$, bandwidth $\Delta\nu = \Delta\omega/2\pi = 37.5\text{ GHz}$, and RMS phase difference between any two coherently combined tiles $\Delta\phi_{RMS} = 2\pi/6$. We consider the lineshape to be Lorentzian. These parameters give a fractional bandwidth of $\Delta\omega/\omega_0 \approx 1.3\times10^{-4}$ and a coherence time of $t_c \approx 8.5\times10^{-12}\text{sec}$. We consider three levels of atmospheric turbulence, $C_n^2 = 0$, $C_n^2 = 10^{-14}\text{m}^{-2/3}$, and $C_n^2 = 10^{-13}\text{m}^{-2/3}$, corresponding to vacuum, moderate turbulence and strong turbulence respectively. Using the Rytov variance, $\sigma_R^2 = 10.5C_n^2\lambda_0^{-7/6}L^{11/6}$, as a measure of turbulence strength, these conditions correspond to $\sigma_R^2 = 0$, $\sigma_R^2 = 6.3$, and $\sigma_R^2 = 63$. We use the Fried parameter, $r_0 = .184\left(C_n^2 L/\lambda_0^2\right)^{-3/5}$, as a measure of the transverse coherence length. Strictly speaking, r_0 corresponds to the diameter of a circular area in which the RMS phase of a plane wave is 1 radian.

a) Vacuum

To observe effects exclusively associated with the linewidth of the laser sources, we begin by considering propagation in vacuum corresponding to $C_n^2 = 0$, $\sigma_R^2 = 0$, and $r_0 = \infty$. Figure 2 displays the intensity profiles at $z = 5\text{ km}$ for the incoherently combined beam (a), coherently combined beam (b), and monochromatic, phase matched beam (c). The intensity profiles are averaged over a time scale much greater than the coherence time, specifically 6 ns. The incoherently combined tiles diffract independently resulting in a radially symmetric, approximately Gaussian intensity profile. The energy from the incoherently combined beam is spread over a much larger area than for the coherently combined beams. The coherently combined beam produces a far field intensity pattern similar to the monochromatic beam. However, there are considerable differences. The coherently combined beam has diffracted more than the monochromatic beam which results in more beam spreading and a lower on axis intensity.

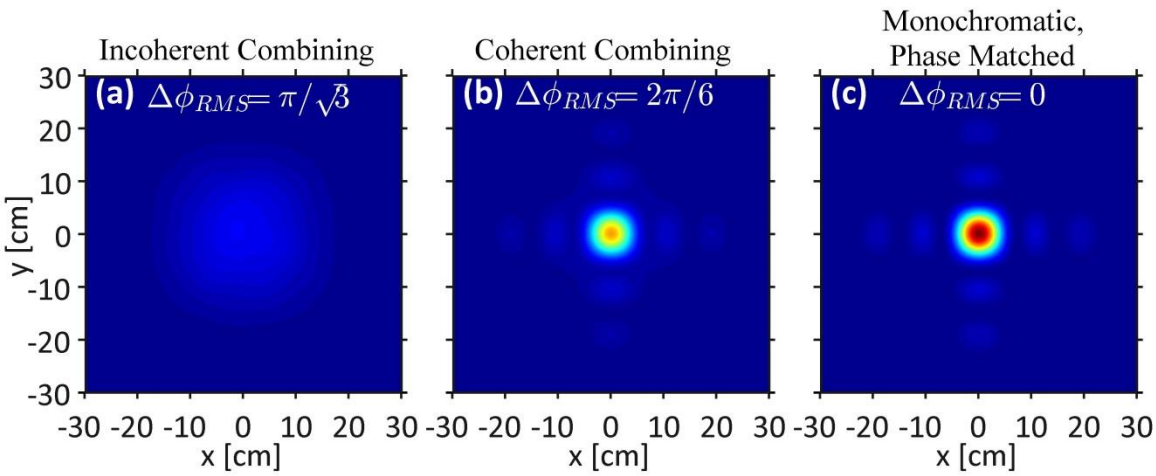

Figure 2: Intensity profiles for propagation through vacuum at $z = 5$ km for the incoherently combined beam (a), coherently combined beam (b), and phase matched monochromatic beam (c). Each tile of the incoherently combined beam diffracts independently resulting in significant spreading. The coherently combined beam has an initial RMS phase difference $\Delta\phi_{RMS} = 2\pi/6$ between any two tiles. The far-field intensity profile of the coherently combined beam resembles that of the monochromatic beam.

Figure 3 displays the intensity profile along the transverse x-axis for the incoherent beam (blue), coherent beam (green), and monochromatic, phase matched beam (red). Intensity is normalized by the on-axis intensity of the monochromatic, phase matched beam. The on axis intensity of the coherently combined beam is approximately 6.4 times greater than the on-axis intensity of the incoherently combined beam. However, the decrease in on-axis intensity of the coherently combined beam in comparison to the monochromatic beam is a fundamental limitation caused by the random temporal characteristics of the phase associated with each individual tile.

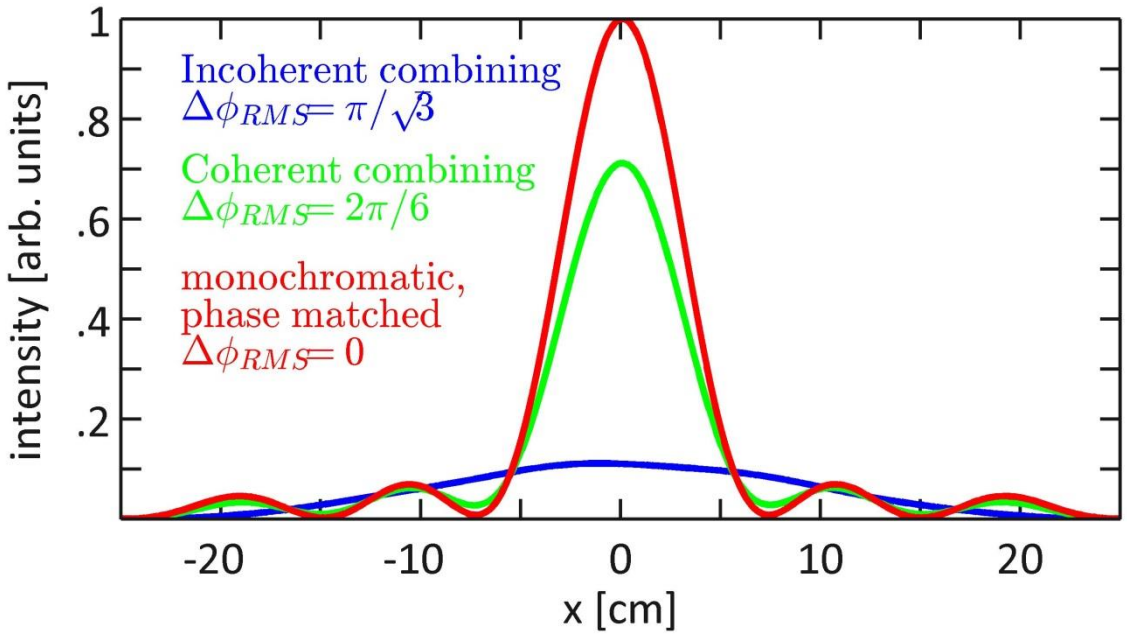

Figure 3: Vacuum intensity profiles along x-axis at $z = 5$ km for the incoherently combined beam (blue), coherently combined beam (green), and phase matched monochromatic beam (red). Intensity is normalized by the on-axis intensity of the monochromatic beam. The on axis intensity of the incoherently and coherently combined beams are approximately 11% and 71% of the on-axis intensity of the monochromatic beam respectively.

A common metric used in DE applications is power in the bucket (PIB), which describes the amount of power contained in a specific area. We calculate the PIB centered at the origin as a function of bucket radius for the time averaged intensity profiles. The results are displayed in Fig. 4 where the PIB is normalized by the total power. Again, incoherent, coherent, and monochromatic results are denoted by blue, green, and red respectively. The coherently combined beam and monochromatic beam each have a distinct central lobe with a radius of approximately 7.5 cm. At a radius of 7.5 cm, the incoherent and coherently combined beams contain 37% and 78%, respectively, of the power contained by the monochromatic beam. Unlike the coherently combined and monochromatic beam, the incoherently combined beam remains radially symmetric at radii greater than the central lobe radius. Consequently, the PIB of the incoherently combined beam increases more rapidly than coherently combined beam after a radius of 7.5 cm. At a radius of 20 cm, the contained power is approximately equal for all beams.

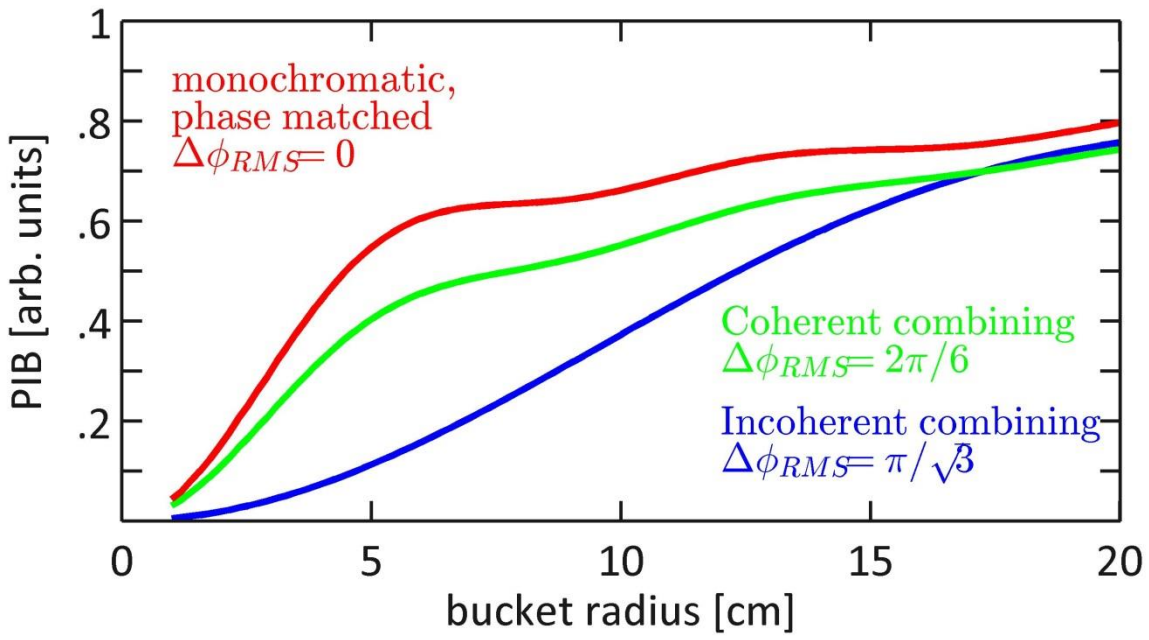

Figure 4: : Power in the bucket (PIB) at $z = 5$ km through vacuum as a function of bucket radius for the incoherently combined beam (blue), coherently combined beam (green), and phase matched monochromatic beam (red). The coherently combined beam and monochromatic beam contain significantly more power near the axis due to the distinct central lobe. The contained power within a radius of 20 cm is approximately equal for all beams.

b) Moderate turbulence

Now we consider propagation through moderate turbulence corresponding to $C_n^2 = 10^{-14}$ m$^{-2/3}$, $\sigma_R^2 = 6.3$, and $r_0 = 1.76$ cm. All other parameters remain the same. An ensemble average is performed over the intensity profiles from 100 independent instances of turbulence. The intensity profile for each instance of turbulence is averaged over many coherence time intervals, 6 ns, to account for the fluctuating intensity and phase. The average intensity profiles at $z = 5$ km are displayed in Fig. 5 for the incoherently combined beam (a), coherently combined beam (b), and phase matched, monochromatic beam (c). Through comparison of the average intensity profiles we can observe a slight advantage of coherent beam combining over incoherent beam combining. These advantages include a smaller spot size and higher maximum intensity. However, the effects of coherent beam combining are nearly insignificant when compared to the impact of moderate turbulence as shown in Fig. 6.

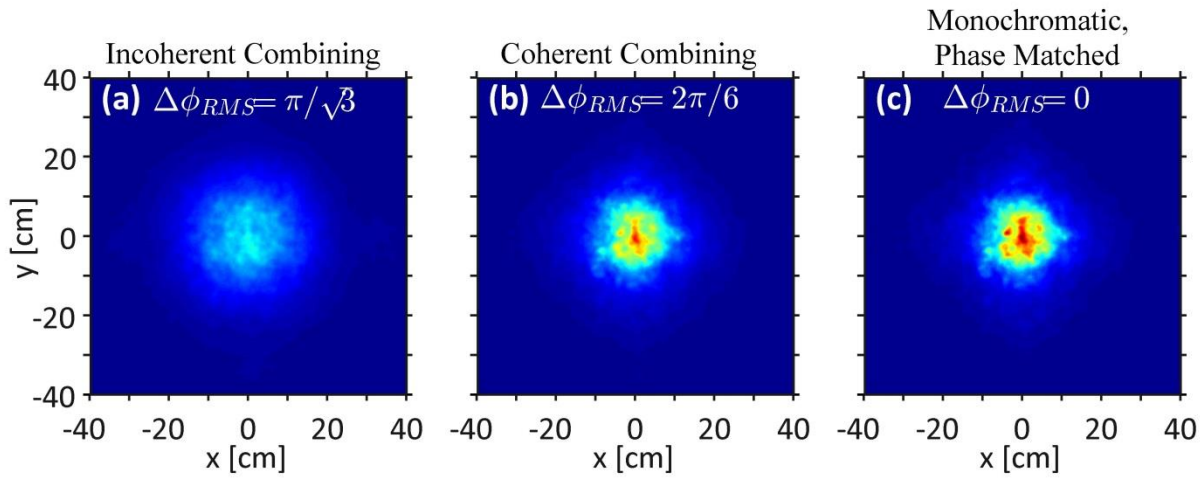

Figure 5: Intensity profiles for propagation through moderate turbulence, $C_n^2 = 10^{-14}$ m$^{-2/3}$, at $z = 5$ km for the incoherently combined beam (a), a coherently combined beam (b), and phase matched monochromatic beam (c). The coherently combined beam and monochromatic beam have smaller spot size and higher on-axis intensity than the incoherently combined beam.

Figure 6 displays the intensity profile along the x-axis for the incoherent (blue), coherent (green), and monochromatic (red) beam profiles. Again, the intensity is normalized by the on-axis intensity of the monochromatic beam in vacuum (black). The on-axis intensity of the coherently combined beam in moderate turbulence is approximately 25% of the on-axis intensity of the coherently combined beam in vacuum. Turbulence has a profound impact on the coherently combined beam in comparison to the incoherently combined beam. The on-axis intensity of the incoherently combined beam in moderate turbulence is approximately 78% of the on-axis intensity of the incoherently combined beam in vacuum.

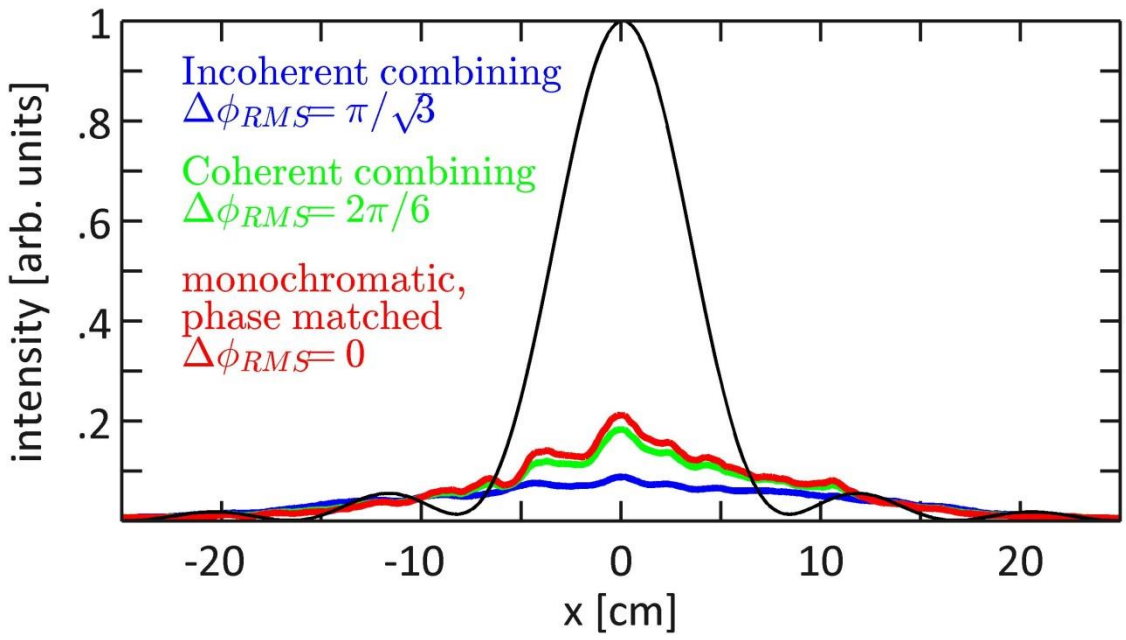

Figure 6: Average intensity profiles in moderate turbulence, $C_n^2 = 10^{-14}$ m$^{-2/3}$, along x-axis at $z = 5$ km for the incoherently combined beam (blue), coherently combined beam (green), and phase matched monochromatic beam (red). Intensity is normalized by the on-axis intensity of a monochromatic beam propagated through vacuum. Propagation through vacuum is denoted by the black curve. The on-axis intensity of the coherently combined is approximately twice the on-axis intensity of the incoherently combined beam.

We also find that moderate turbulence significantly impacts the advantage of PIB for coherently combined beam. Figure 7 displays the PIB as a function of radius at $z = 5$ km for beams propagating through moderate turbulence. The coherently combined beam and monochromatic beam no longer have a distinct central lobe as in the case of propagation through vacuum. As a result, the PIB of each beam has a similar trend. The coherently combined beam and monochromatic beam still contain more power near the axis than the incoherently combined beam, but the difference is not as significant. The advantage of coherent combining appears minor when compared to the PIB to a phase matched, monochromatic beam in vacuum. Even in moderate turbulence, it is clear that the phase distortions caused by atmospheric turbulence are dominant over the effects of coherent beam combining.

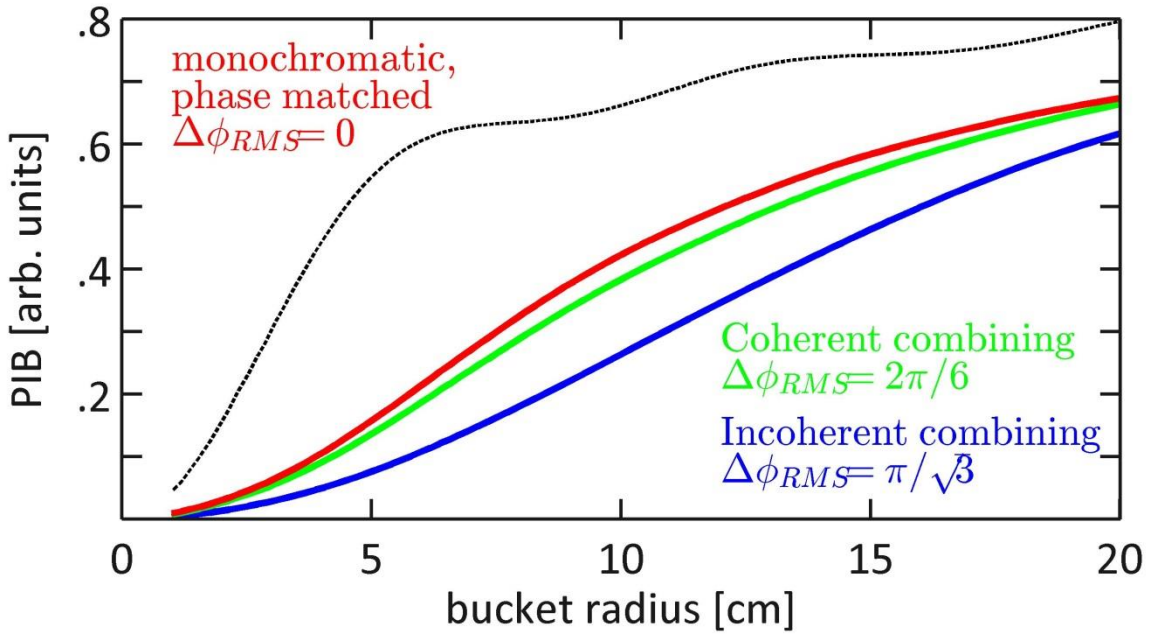

Figure 7: Power in the bucket (PIB) at $z = 5$ km through moderate turbulence, $C_n^2 = 10^{-14}$ m$^{-2/3}$, as a function of bucket radius for the incoherently combined beam (blue), coherently combined beam (green), and phase matched monochromatic beam (red). For reference, the PIB of the monochromatic, phase matched beam propagated through vacuum is denoted by the dashed black curve. The coherently combined beam and monochromatic beam contain more power near the axis than the incoherently combined beam, however the difference is not as significant as in vacuum.

c) Strong turbulence

Finally, we consider propagation through strong turbulence corresponding to $C_n^2 = 10^{-13}$ m$^{-2/3}$, $\sigma_R^2 = 63$, and $r_0 = .44$ cm. All other parameters remain the same. Again, an ensemble average is performed over the intensity profiles associated with 100 independent instances of turbulence and the intensity profile for each instance of turbulence is averaged over 6 ns. The average intensity profiles at $z = 5$ km are displayed in Fig. 8 for the incoherently combined beam (a), coherently combined beam (b), and phase matched, monochromatic beam (c). All three intensity profiles are nearly indistinguishable from each other. The intensity profiles of the coherently combined beam and monochromatic beam have no resemblance to the vacuum far-field pattern displayed in Fig. 2b,c.

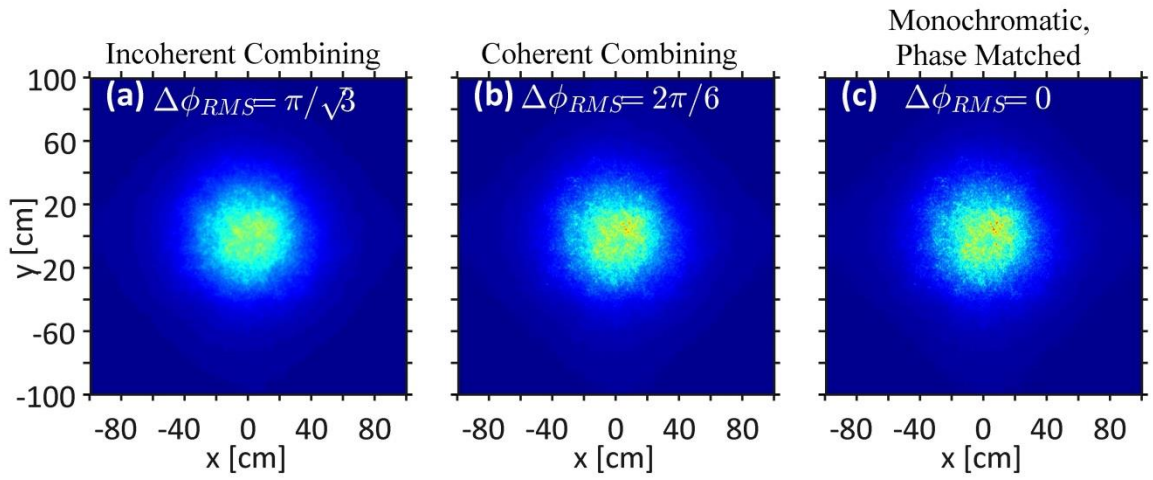

Figure 8: Intensity profiles for propagation through strong turbulence, $C_n^2 = 10^{-13}$ m$^{-2/3}$, at $z = 5$ km for the incoherently combined beam (a), coherently combined beam (b), and phase matched monochromatic beam (c). The intensity profiles are nearly indistinguishable.

Figure 9 displays the intensity profile along the x-axis for the incoherent beam (blue), coherent beam (green), and monochromatic beam (red). Again, the intensity is normalized by the on-axis intensity of the monochromatic beam in vacuum. Atmospheric turbulence is dominant over the method of beam combining; consequently, the shape of each intensity profile is nearly identical. The main noticeable difference is that the coherently combined beam and monochromatic beam have slightly higher spatial fluctuations in the time averaged intensity.

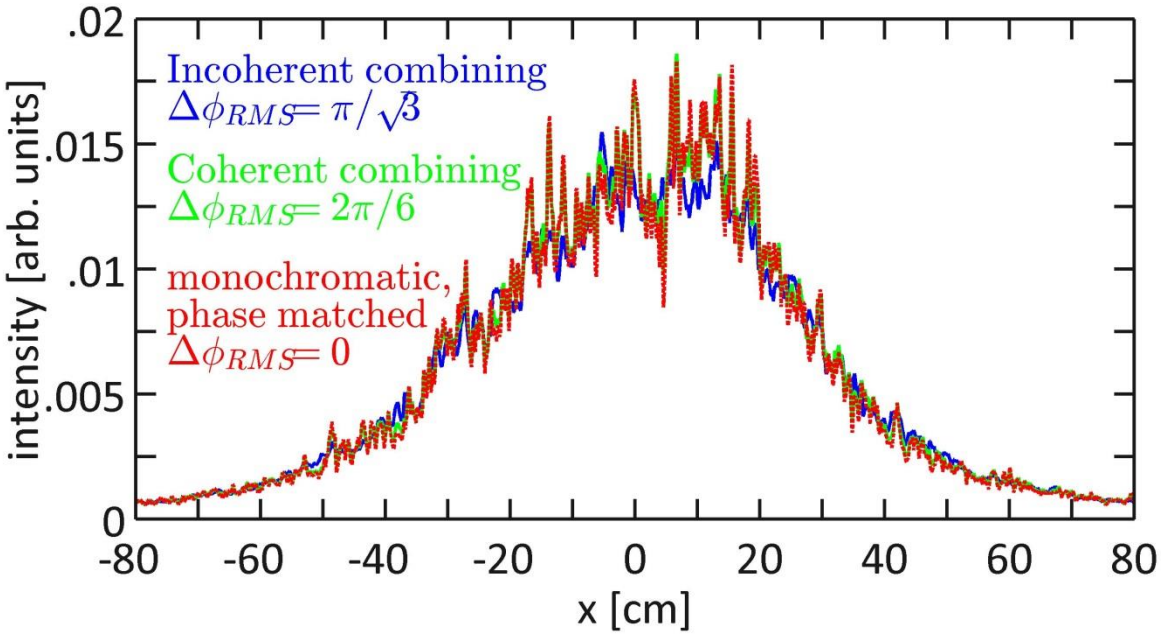

Figure 9: Intensity profiles in strong turbulence, $C_n^2 = 10^{-13}$ m$^{-2/3}$, along x-axis at $z = 5$ km for the incoherently combined beam (blue), coherently combined beam (green), monochromatic beam (red). Intensity is normalized by the on-axis intensity of a monochromatic beam in vacuum. The intensity profiles are nearly indistinguishable.

Figure 10 displays the PIB as a function of radius for the incoherent beam (blue), coherent beam (green), and monochromatic beam (red). The initial condition of the phase at $z = 0$ has very little discernible impact on the PIB at $z = 5$ km in strong turbulence. The advantages of coherent beam combining that were apparent in vacuum have completely diminished in strong turbulence.

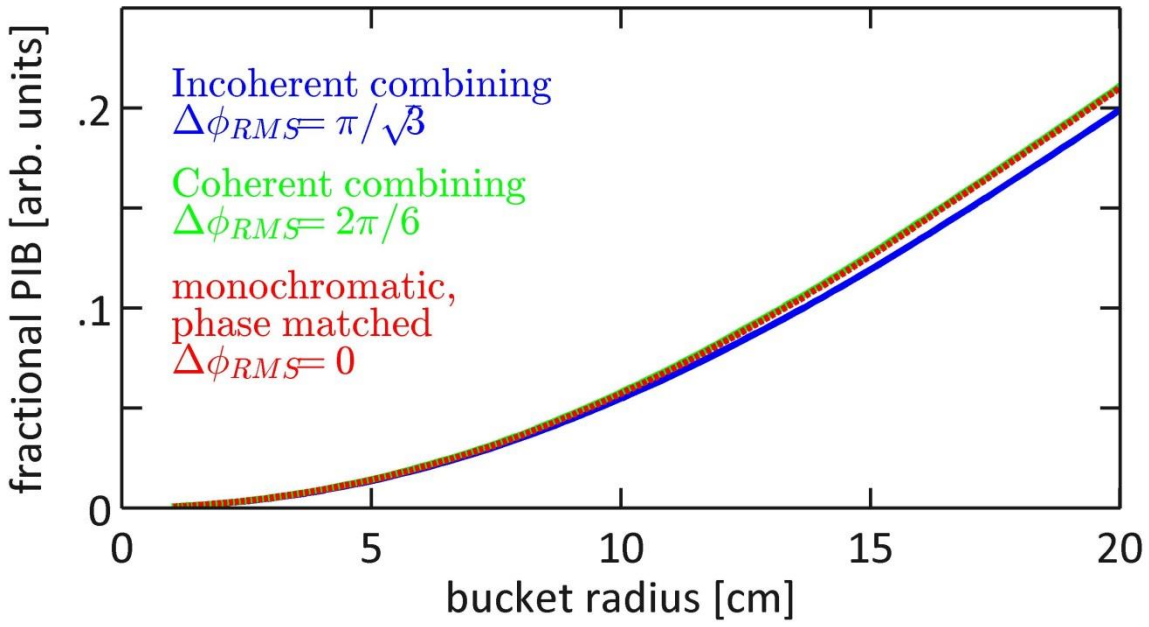

Figure 10: Power in the bucket (PIB) at $z = 5$ km through strong turbulence, $C_n^2 = 10^{-13}$ m$^{-2/3}$, as a function of bucket radius for the incoherently combined beam (blue), coherently combined beam (green), and phase matched monochromatic beam (red). All beams deliver approximately the same power.

IV. Discussion

We have demonstrated that the linewidth of the source places a fundamental limit on the ability to coherently combine beams. The large linewidth associated with high-power lasers must be carefully considered if they are to be coherently combined. However, coherently combining beams at the transmitter plane has no benefit for DE systems in conditions of strong turbulence. We have shown that the initial RMS phase difference between tiles has negligible impact on the quality of the beam after propagation through multiple kilometers of moderate or strong atmospheric turbulence. In strong turbulence, coherent beam combining at the transmitter plane merely adds to the complexity of the transmitter. Situations of strong turbulence and multi-km distances require adaptive optics to compensate for the phase distortions caused by atmospheric turbulence. Depending on the implementation of the adaptive optics, the linewidth of high-power lasers may need to be taken into consideration. For instance, coherent combining at the target can be considered an adaptive optics method because it partially compensates for distortions caused

by atmospheric turbulence. In this case, the linewidth of high-power lasers places even greater limitations on coherent combining due to the transit time of light to the target and back to the receiver. If the transit time is longer than the coherence time of the lasers, then it is inconceivable to coherently combine the lasers at the target without first phase matching the beams at the transmitter.

There are multiple limitations that the linewidth of a laser places on the ability to coherently combine beams. Due to the dominant effect of atmospheric turbulence, it is not effective to coherently combine lasers at the transmitter plane. Incoherent combining of lasers is a much simpler approach with comparable results in moderate to strong turbulence. A more effective approach for delivering energy to a target in moderate to strong turbulence may be in using adaptive optics solutions to compensate for the turbulent distortions.

Acknowledgements

This work was supported by funding from JTO, through ONR under Contract No. N000141211029 and by the Naval Research Laboratory.

References

[1] Ellis, J. D. “Directed-Energy Weapons: Promise and Prospects” (CNAS, 2015).

[2] G. D. Goodno, C. P. Asman, J. Anderegg, S. Brosnan, E. C. Cheung, D. Hammons, H. Injeyan, H. Komine, W. Long, M. McClellan, S. J. McNaught, S. Redmond, R. Simpson, J. Sollee, M. Weber, S. B. Weiss, and M. Wickham, “Brightness-scaling potential of actively phase-locked solid state laser arrays,” IEEE J. Sel. Topics Quantum Electron., vol. 13, no. 3, pp. 460–472, May/Jun. 2007.

[3] P. Zhou, Z. Liu, X. Wang, Y. Ma, H. Ma, X. Xu, and S. Guo, “Coherent beam combining of fiber amplifiers using stochastic parallel gradient descent algorithm and its application,” IEEE J. Sel. Topics Quantum Electron., vol. 15, no. 2, pp. 240–247, Mar.–Apr. 2009.

[4] T. Weyrauch, M. A. Vorontsov, G. W. Carhart, L. A. Beresnev, A. P. Rostov, E. E. Polnau, and J. J. Liu, “Experimental demonstration of coherent beam combining over a 7 km propagation path,” Opt. Lett. 36, 4455–4457 (2011).

[5] G. D. Goodno, S. J. McNaught, J. E. Rothenberg, T. S. Mccomb, P. A. Thielen, M. G. Wickham, and M. E. Weber, “Active phase and polarization locking of a 1.4 kW fiber amplifier,” Opt. Lett. 35, 1542–1544 (2010).

[6] P. Sprangle, A. Ting, J. Peñano, R. Fischer, B. Hafizi, “Incoherent Combining and Atmospheric Propagation of High-Power Fiber Lasers for Directed-Energy Applications” IEEE J. Quant. Elec., 45(2), 138-148 (2009).

[7] P. Sprangle , J. Peñano, B. Hafizi and A. Ting "Incoherent combining of high-power fiber lasers for long-range directed energy applications", J. Directed Energy, vol. 2, pp.273 -284 (2007).

[8] P. W. Milonni and J. H. Eberly, Laser Physics (Wiley, 2010).

[9] L. Mandel, E. Wolf, *Optical Coherence and Quantum Optic,* Cambridge University Press, (1995).

[10] N. Ruggieri, D. Cummings, G. Lachs, “Simulation of superposed coherent and chaotic radiation of arbitrary spectral shape”, J. Appl. Phys. 43(3), (1972).

[11] G. Vannucci and M. C. Teich, “Computer simulation of superposed coherent and chaotic radiation”, App. Opt. 19(4), (1980).

[12] W. Nelson, J. P. Palastro, C. C. Davis, and P. Sprangle, “Propagation of Bessel and Airy beams through atmospheric turbulence,” J. Opt. Soc. Am. A 31, 603–609 (2014).

Appendix A

For a continuous power spectrum of radiation, $\sigma^2(\omega)$, the variance of a_n and b_n in Eq. (1) are $\mathrm{Var}(a_n) = \mathrm{Var}(b_n) = \delta\omega\sigma^2(\omega_n)$. Here we consider a Gaussian power spectrum, σ_G^2, and a Lorentzian power spectrum, σ_L^2, defined as

$$\sigma_G^2(\omega) = \frac{1}{\Gamma_G\sqrt{2\pi}}\exp\left(\frac{-(\omega-\omega_0)^2}{2\Gamma_G^2}\right), \tag{A1}$$

$$\sigma_L^2(\omega) = \frac{1}{\pi}\left[\frac{\Gamma_L}{(\omega-\omega_0)^2+\Gamma_L^2}\right] \tag{A2}$$

respectively, where Γ_G and Γ_L are parameters that determine the width of each power spectrum. The power spectra are normalized such that

$$\int_{-\infty}^{+\infty}\sigma_G^2(\omega)\,d\omega = \int_{-\infty}^{+\infty}\sigma_L^2(\omega)\,d\omega = 1. \tag{A3}$$

The linewidth, $\Delta\omega$, is defined as the full width at half maximum (FWHM) of the power spectrum. The FWHM of a Gaussian function is defined as $\Delta\omega_G = 2(2\ln 2)^{1/2}\Gamma_G$ and the FWHM of a Lorentzian function is defined as $\Delta\omega_L = 2\Gamma_L$. For comparison of the two spectra, it is convenient to pick Γ_G and Γ_L such that $\Delta\omega_G = \Delta\omega_L = \Delta\omega$. For example, $\Gamma_G = 100\mathrm{GHz}$ and $\Gamma_L = (2\ln 2)^{1/2}\Gamma_G = 117.7\mathrm{GHz}$ which gives the relation $\Delta\omega_G = \Delta\omega_L = \Delta\omega = 235.5\mathrm{GHz}$. The coherence time is defined as $t_c = 2/\Delta\omega$. The linewidth ratio for this example is $\Delta\omega/\omega_0 = 1.24\times10^{-4}$. Figure A1 displays a comparison of two power spectra for these parameters.

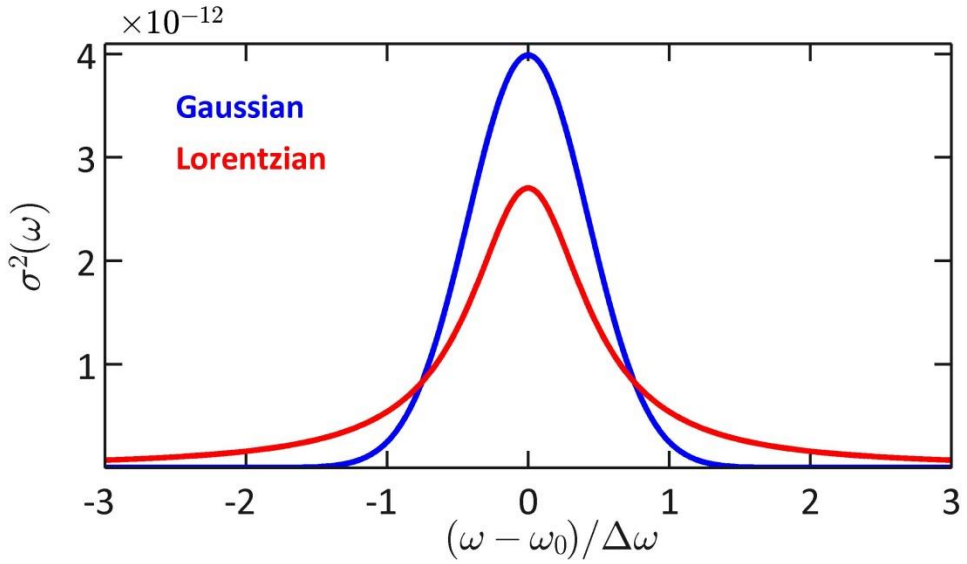

Figure A1: Comparison of a Gaussian and Lorentzian power spectrum when the linewidths are matched, i.e. $\Delta\omega_G = \Delta\omega_L = \Delta\omega$. The Gaussian power spectrum contains 98% of the total power within $\Delta\omega$ of ω_0. The Lorentzian power spectrum contains 70% of the total power within $\Delta\omega$ of ω_0.

The Lorentzian power spectrum decays more slowly than the Gaussian power spectrum and thus a greater fraction of the total power is contained at frequencies far from ω_0. For example, the Gaussian power spectrum contains 98% of the total power within $\Delta\omega$ of ω_0, while the Lorentzian power spectrum contains 70% of the total power within $\Delta\omega$ of ω_0. Appendix B illustrates this importance by comparing the random fluctuations in the intensity and phase for Gaussian and Lorentzian power spectral densities.

Appendix B

Here we illustrate the random fluctuations in the intensity and phase. We examine the behavior of the intensity and phase for a single tile at $z = 0$ and on time scales comparable to the coherence time, t_c. The intensity of a tile is defined as

$$I(t) = \frac{c}{4\pi}\left\langle E(t)^2 \right\rangle_{t=2\pi/\omega_0} = \frac{c}{8\pi}\left(\alpha^2(t) + \beta^2(t)\right), \qquad \text{(B1)}$$

where the angled brackets indicate a temporal average performed over a time scale of $2\pi/\omega_0$. It is convenient to define a normalized intensity as $I_0(t)=\alpha^2(t)+\beta^2(t)$. Due to the statistical properties of α and β we have the relation $\langle I_0(t)\rangle_{t\gg t_c}\approx 1$. The phase of a tile is defined as

$$\phi(t)=\arctan\left[\beta(t)/\alpha(t)\right]. \tag{B2}$$

We note that strictly speaking, the arctan function has a range of $(-\pi/2,\pi/2)$. Numerically, we utilize the atan2 function so that the phase of a tile is defined on the interval $(-\pi,\pi]$.

We begin by considering a tile with a Gaussian power spectrum defined by Eq. (A1). Figure B1 shows the intensity fluctuations at $z=0$ for a single tile with a Gaussian power spectrum. The intensity fluctuates randomly, but still appears as a smooth function in time. Major fluctuations occur over intervals greater than the coherence time as displayed in figure Fig. B1. Calculating the long term average intensity for this specific instance of α and β gives the result $\langle I_0(t)\rangle_{t=750t_c}\approx 1.01$.

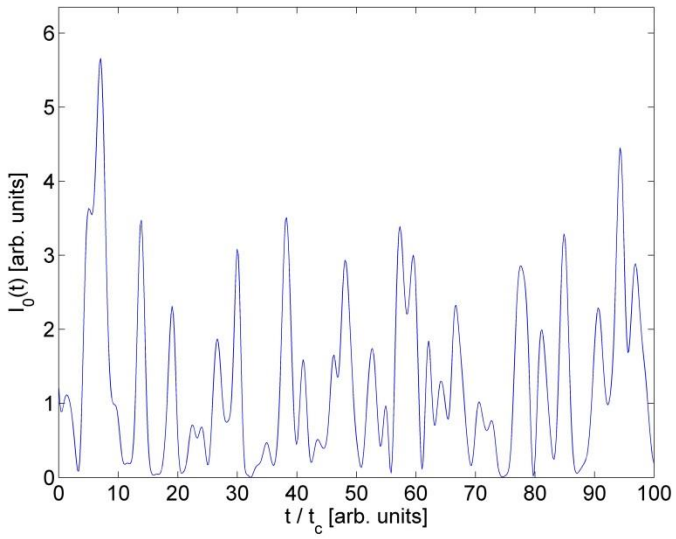

Figure B1: Intensity fluctuations for a single tile with Gaussian power spectrum. The intensity has random fluctuations when observed on time scales comparable to the coherence time. The standard deviation of intensity is equal to the average intensity.

Figure B2 shows the phase fluctuations at $z=0$ for a single tile with a Gaussian power spectrum. Similar to the intensity, the phase fluctuates randomly when observed on a time scale comparable to the coherence time.

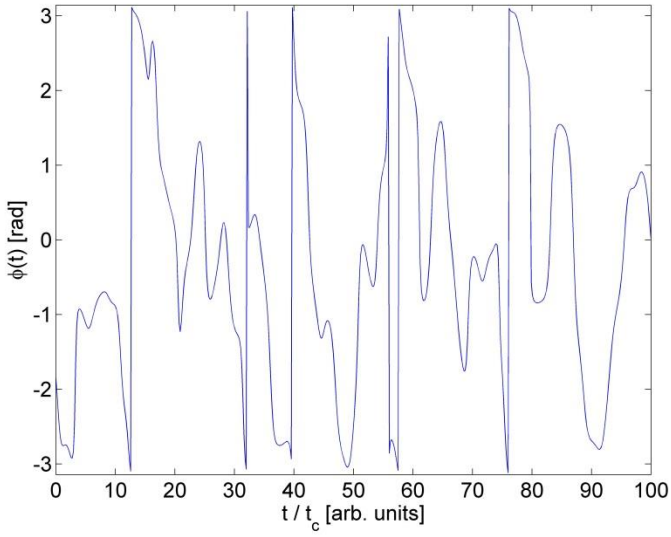

Figure B2: Phase fluctuations for a single tile with Gaussian power spectrum. The phase fluctuates randomly when observed on time scales comparable to the coherence time.

The intensity and phase as a function of time is characteristically different when the tile has a Lorentzian power spectrum described by Eq. (A2). Figure B3 shows the intensity fluctuations at $z = 0$ for a single tile with a Lorentzian power spectrum. Similar to the case of the Gaussian power spectrum, large scale fluctuations occur over times of a few coherence time intervals. However the intensity fluctuations do not appear as a smooth function. Regardless, performing a long time average gives the result $\langle I_0(t) \rangle_{t=750t_c} \approx .98$, which is close to the expected value of 1.

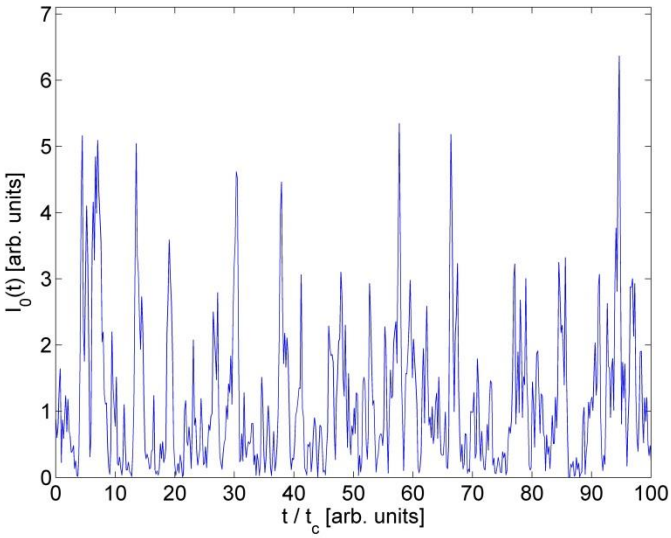

Figure B3: Intensity fluctuations for a single tile with a Lorentzian power spectrum. The standard deviation of intensity is equal to the average intensity.

Figure B4 shows the phase fluctuations at $z = 0$ for a single tile with a Lorentzian power spectrum. The phase displays the same random fluctuations over time scales comparable to the coherence time.

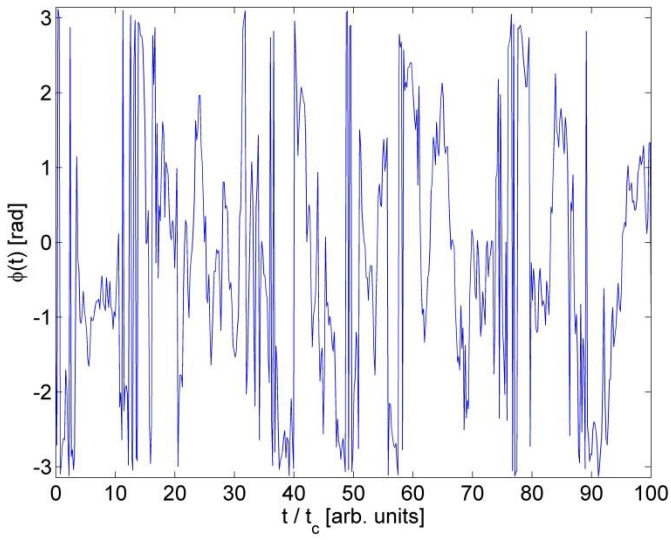

Figure B4: Phase fluctuations for a single tile with a Lorentzian power spectrum.

Appendix C

Ideally, the phase of two coherently combined beams would fluctuate synchronously and have a phase difference of zero at any instance in time. However, in practice this is generally not the case, especially for high-power lasers. Instead, coherent combining systems result in a reduction of the root mean square (RMS) phase difference between beams. To simulate a situation where the tiles are coherently combined in the transmitter plane, we develop a method to generate a set of $\alpha_{l,m}(t)$ and $\beta_{l,m}(t)$ in which the RMS phase difference between any two tiles can be controlled. As an illustration, we consider 2 tiles whose amplitude and phase are modulated by $\alpha_1(t)$, $\beta_1(t)$, $\alpha_2(t)$, and $\beta_2(t)$. These variables are generated through the Fourier transform of the Gaussian random variables $a_n^{(1)}, b_n^{(1)}, a_n^{(2)}, b_n^{(2)}$ where we have added the superscript to distinguish between tiles. If we assume that perfect coherent combining is implemented for all frequency components within a certain frequency bandwidth, $|\omega_n - \omega_0| < \Omega$, where Ω is the half width of the coherent combining instrument bandwidth, then $a_n^{(1)} \equiv a_n^{(2)}$ and $b_n^{(1)} \equiv b_n^{(2)}$ for $|n| < \Omega/\delta\omega$. In other words, random variables associated with frequency components contained within the coherent combining bandwidth are shared between the tiles. Conversely, random variables associated with

frequency components outside of the coherent combining bandwidth are uncorrelated between the tiles. The coherent combining bandwidth is determined by the time scale over which the coherent combining instruments operate. We assume that the instruments have zero error and thus can precisely phase match all frequency components within the instrument bandwidth.

We define ϕ_1, ϕ_2 and $\Delta\phi$ as the phase of tile 1, phase of tile 2, and the phase difference between the two tiles respectively. In terms of $\alpha_1(t)$, $\beta_1(t)$, $\alpha_2(t)$, and $\beta_2(t)$ we have the relations

$$\phi_1(t) = \arctan\left[\beta_1(t)/\alpha_1(t)\right] \quad , \tag{C1}$$

$$\phi_2(t) = \arctan\left[\beta_2(t)/\alpha_2(t)\right] \quad , \tag{C2}$$

$$\Delta\phi(t) = \left|\phi_1(t) - \phi_2(t)\right| \quad . \tag{C3}$$

The RMS phase difference between the two tiles is defined as:

$$\Delta\phi_{RMS} = \left(\frac{1}{N}\sum_t \Delta\phi^2(t)\right)^{1/2} . \tag{C4}$$

We can analytically calculate $\Delta\phi_{RMS}$ for the cases of incoherently combined tiles and perfectly phase matched tiles. If the two tiles are incoherently combined, then $\Delta\phi$ is a random variable with a uniform distribution on the interval $[0,\pi]$ and $\phi_{rms} = \mathrm{E}\left[\Delta\phi^2\right]^{1/2}$. From the properties of a uniform distribution we know the expected value, $\mathrm{E}[\Delta\phi] = \pi/2$, and variance, $\mathrm{Var}[\Delta\phi] = \pi^2/12$. Using the definition of variance, $\mathrm{Var}[X] = \mathrm{E}\left[X^2\right] - \mathrm{E}[X]^2$, we calculate $\mathrm{E}\left[\Delta\phi^2\right] = \pi^2/3$ and $\Delta\phi_{RMS} = \pi/\sqrt{3}$. On the other hand, if the two tiles are perfectly phase matched then $\Delta\phi$ is uniquely zero and clearly $\Delta\phi_{RMS} = 0$. These simple situations of incoherent combining and perfect phase matching correspond to $\Omega = 0$ and $\Omega = \infty$ respectively. Coherently combining monochromatic sources is an example of perfect phase matching. We calculate intermediary values $\Delta\phi_{RMS}(\Omega)$ for both Gaussian and Lorentzian power spectra displayed in Fig. C1.

For a Gaussian power spectrum, the RMS phase difference between the two tiles is effectively zero when frequency components within $\Omega = 2\Delta\omega$ of ω_0 are matched. However, the result differs greatly when the two tiles have a Lorentzian power spectrum. Since a higher percentage of power is contained at frequencies far from ω_0, $\Delta\phi_{RMS}(\Omega)$ decays much slower. From Fig. C1, it is clear that it becomes very difficult to achieve a small RMS phase difference between two tiles with a Lorentzian power spectrum.

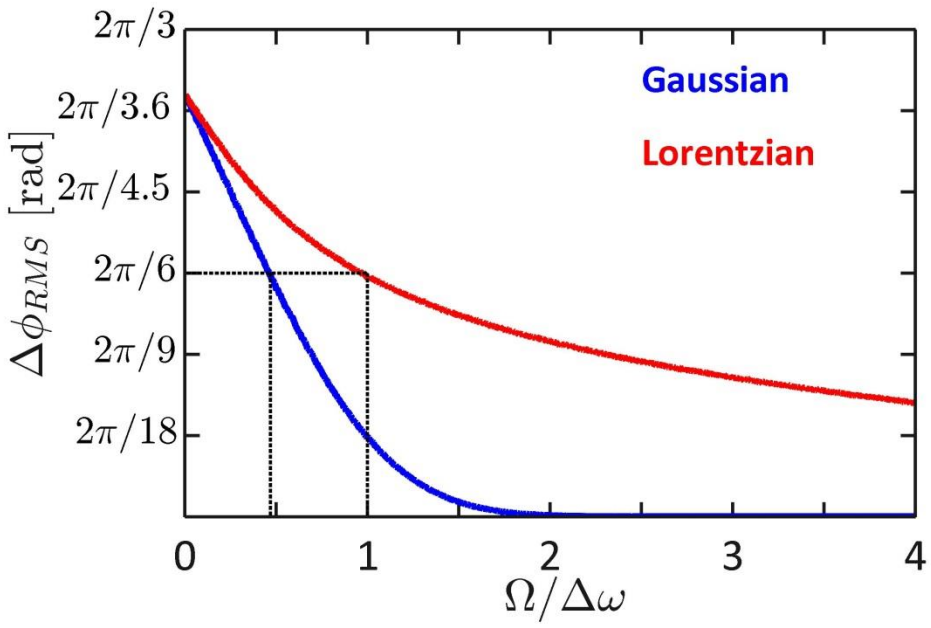

Figure C1: The RMS phase difference between two tiles with a Gaussian power spectrum (blue) and Lorentzian power spectrum (red) as a function of instrument bandwidth.

Recalling that Ω is the half width of the coherent combining angular frequency bandwidth, we can use Fig. C1 to calculate the rate at which the instruments must operate to achieve any arbitrary RMS phase. For example, to achieve coherent beam combining with an RMS phase difference of $2\pi/6$ would require instruments that operate at a rate of $2(.48\Delta\omega)/2\pi \approx 36$ GHz and $2\Delta\omega/2\pi = 75$ GHz for a Gaussian and Lorentzian linewidth respectively. In the following simulations, we consider the propagation of coherently combined beams with a Lorentzian power spectrum.